BIOCHEMISTRY
including biophysical chemistry & molecular biology

Article

pubs.acs.org/biochemistry

The Loss of an Electrostatic Contact Unique to AMPA Receptor Ligand Binding Domain 2 Slows Channel Activation

Sandra M. Holley,[†,§] Ahmed H. Ahmed,[†] Jayasri Srinivasan,[†] Swetha E. Murthy,[‡] Gregory A. Weiland,[†] Robert E. Oswald,[†] and Linda M. Nowak*[,†]

[†]Department of Molecular Medicine, Cornell University, Ithaca, New York 14853, United States

[‡]Department of Biochemistry, University at Buffalo, Buffalo, New York 14214, United States

Supporting Information

ABSTRACT: Ligand-gated ion channels undergo conformational changes that transfer the energy of agonist binding to channel opening. Within ionotropic glutamate receptor (iGluR) subunits, this process is initiated in their bilobate ligand binding domain (LBD) where agonist binding to lobe 1 favors closure of lobe 2 around the agonist and allows formation of interlobe hydrogen bonds. AMPA receptors (GluAs) differ from other iGluRs because glutamate binding causes an aspartate−serine peptide bond in a flexible part of lobe 2 to rotate 180° (flipped conformation), allowing these residues to form cross-cleft H-bonds with tyrosine and glycine in lobe 1. This aspartate also contacts the side chain of a lysine residue in the hydrophobic core of lobe 2 by a salt bridge. We investigated how the peptide flip and electrostatic contact (D655−K660) in GluA3 contribute to receptor function by examining pharmacological and structural properties with an antagonist (CNQX), a partial agonist (kainate), and two full agonists (glutamate and quisqualate) in the wildtype and two mutant receptors. Alanine substitution decreased the agonist potency of GluA3$_i$-D655A and GluA3$_i$-K660A receptor channels expressed in HEK293 cells and differentially affected agonist binding affinity for isolated LBDs without changing CNQX affinity. Correlations observed in the crystal structures of the mutant LBDs included the loss of the D655−K660 electrostatic contact, agonist-dependent differences in lobe 1 and lobe 2 closure, and unflipped D(A)655−S656 bonds. Glutamate-stimulated activation was slower for both mutants, suggesting that efficient energy transfer of agonist binding within the LBD of AMPA receptors requires an intact tether between the flexible peptide flip domain and the rigid hydrophobic core of lobe 2.

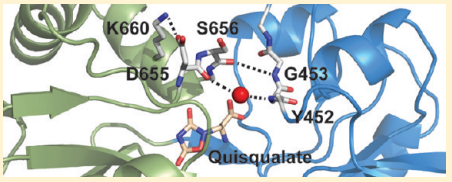

Glutamate mediates excitatory synaptic transmission in brain by activation of AMPA (GluA1−4), kainate (GluK1−5), and NMDA (GluN1−3) receptors. The molecular diversity of the ionotropic glutamate receptor (iGluR) subfamilies is important for their divergent functional roles. AMPA receptors mediate fast synaptic transmission in the central nervous system, while NMDA channels, with slower activation, high Ca^{2+} permeability, and voltage sensitivity to block by external and internal Mg^{2+} ions, act as coincidence detectors at the synapse[1] and activate transduction mechanisms for nuclear signaling.[2−4] Together, AMPA and NMDA receptors mediate activity-dependent synaptic plasticity underlying learning and memory formation,[5−8] and Ca^{2+}-permeable AMPA channels contribute to excitotoxic cell death in epilepsy, hypoxic ischemia, and neurodegenerative diseases.[8−11] A deeper understanding of AMPA receptor activation will be useful for developing agents to regulate sleep and respiration and to treat some forms of epilepsy and cognitive disorders whose pathological features are related to dysregulation of GluA receptor function.

Knowledge of the conformational changes and molecular rearrangements that contribute to agonist activation of GluA receptors is essential to understanding how drugs might be designed to modify channel function. Detailed structures of the ligand binding domains of iGluRs[12−15] showed that ligands bind in a cleft between the two lobes in the LBD (Figure 1A, GluA3 with quisqualate bound). AMPA receptor LBDs bound to full agonists are closed by 20−22° relative to unliganded apo structures, and there is a 180° rotation around a peptide bond in lobe 2 hypothesized to play a role in receptor activation.[12,16] In this flipped position, there is an additional hydrogen bond between the carbonyl of D655 through a water molecule to the amide of Y452 and another between the carbonyl of S656 and the amide of G453 (Figure 1B). D655 also forms a salt bridge with K660 of GluA3 (Figure 1C). This salt bridge is seen in GluA structures, and as suggested by primary sequences and observed in crystal structures of other iGluR LBDs (Figure 1D), it appears to be unique to AMPA receptors.[14,15,17,18]

The activation of ligand-gated receptors has been described as a wave of conformational changes starting with the initial interaction of the agonist with the receptor and ending in the opening of the channel gate.[19,20] We hypothesized that the D655−K660 salt bridge may contribute to the transmission of the energy of binding of the agonist to channel opening by tethering D655 to helix F in the hydrophobic core of lobe 2 and investigated this by single-alanine substitutions at each residue.

Received: February 8, 2012
Revised: April 4, 2012
Published: April 18, 2012

dx.doi.org/10.1021/bi3001837 | *Biochemistry* 2012, 51, 4015−4027

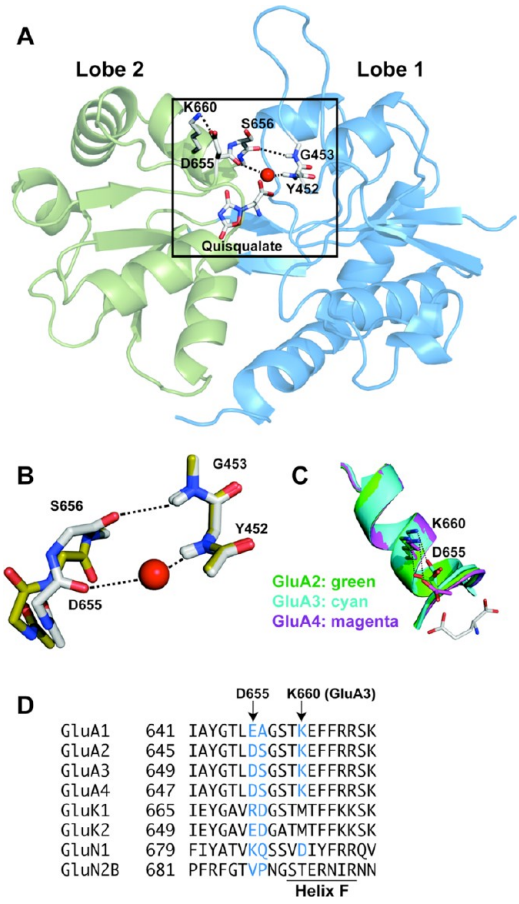

Figure 1. Structural elements of iGluRs. (A) Structure of the $GluA3_o$ LBD with quisqualate bound. The D655−S656 peptide bond is in the flipped form, and the red sphere indicates the position of a water molecule. The ligand-binding site (box) is featured in Figures 7 and 8 and Figure S2 of the Supporting Information. (B) Flipped (white carbon atoms) and unflipped (yellow carbon atoms) forms of the peptide bond illustrate the H-bonds across the lobe interface for the flipped form, which includes one contact through a water molecule. (C) The electrostatic contact between the peptide flip Asp and the Lys residue in helix F tethers the flexible loop to the hydrophobic core in lobe 2 of GluA receptors. The stick representation of glutamate marks the position of the binding site at the end of the helix. (D) Partial sequence alignment of a portion of lobe 2 for a series of AMPA, kainate, and NMDA receptors. Arrows denote the positions mutated in this study (D655A and K660A in GluA3); residues in helix F are marked below.

Comparing wild-type and mutant LBD structures demonstrated the loss of the D655−K660 salt bridge and changes in binding affinity that were ligand-dependent. Electrophysiological analysis revealed increased agonist EC_{50} values (decreased potency), and glutamate response activation was slower for both mutations. Together, these observations provide evidence that the energy of agonist-induced conformational changes in the LBD is transmitted more effectively to the channel when the D655−K660 salt bridge is intact and further support a role for the peptide flip conformational change in AMPA receptor activation.

MATERIALS AND METHODS

Plasmids, Mutations, and Cells. Plasmids for rat wild-type GluA3-*flip* ($GluA3_i$) and two mutant subunits were constructed in the laboratory. Rat wild-type GluA3-*flop* cDNA ($GluA3_o$) (gift of S. Heinemann, Salk Institute, San Diego, CA) was excised from pBluescript and transferred to the pRK5 (Stratagene, La Jolla, CA) mammalian expression vector. The flop sequence was replaced by a flip sequence containing the cyclothiazide (CTZ) binding site and a glycine (G747) residue at the R/G editing site obtained by polymerase chain reaction amplification using GluA3 specific primers in an E14 mouse brain cDNA library (gift of J. Eberwine, University of Pennsylvania, Philadelphia, PA). The blasticidin resistance gene was excised from pE/BSD (Invitrogen, Carlsbad, CA) and transferred to the pRK5/r-$mGluA3_i$ construct into the *Hpa*I site distal to the SV40 polyadenylation sequence. The aspartate to alanine (D655A) and the lysine to alanine (K660A) mutations were made in the pRK5/r-$mGluA3_i$ plasmid using the QuikChange (Stratagene) mutagenesis kit. The pRK5/r-$mGluA3_i$/Bsd, pE/r-$mGluA3_i$-D655A/Neo, and pE/r-$mGluA3_i$-K660A/Neo transfection plasmids were completely sequenced in overlapping reactions performed in both directions (Cornell University BioResource Center, Ithaca, NY).

Three sets of cell lines stably expressing the wild-type $GluA3_i$, $GluA3_i$-D655A,or $GluA3_i$-K660A receptor in human embryonic kidney (HEK293) cells lacking the T antigen (ATCC, Manassas, VA) were used in the majority of experiments. Cells were cotransfected with puromycin expression vector pUR (Clontech, Mountain View, CA) and one of the $GluA3_i$ plasmids in a 1:3 ratio using cationic lipid-based transfection reagents (PolyFect, Qiagen, Valencia, CA; or Lipofectamine 2000, Invitrogen). Eighteen to twenty-four hours later, cells were exposed to 10 μg/mL puromycin (Sigma-Aldrich, St. Louis, MO) for 1−2 h and then washed with FBS-containing DMEM. Surviving cells were challenged with selection antibiotics [20−25 μg/mL blasticidin (Invitrogen) or 1.5−2.5 mg/mL Geneticin (G418)] to establish stable cell lines. Single colonies of cells were isolated and expanded under continuous antibiotic selection. Cell lines expressing 0.3−1 nA glutamate-evoked current per cell in whole cell recordings were frozen (DMEM with 20% FBS and 8.5% DMSO) at −80 °C and used later in recordings. These cells and HEK293T cells (ATCC)[21] were transiently transfected to boost the level of receptor expression for the fast glutamate application experiments in outside-out patches with the appropriate receptor cDNA and the pE/BFP plasmid (Clontech) using the PolyFect reagent (Qiagen) in a 3:1 plasmid ratio (1.8 μg of cDNA/35 mm dish). All cells were cultured and maintained in Dulbecco's modified MEM (Gibco/Invitrogen) supplemented with 10% fetal bovine serum (FBS) (Gemini Bioproducts, West Sacramento, CA).

Electrophysiology. Whole cell patch clamp recordings were performed at room temperature (22−24 °C) as described by Hamill et al.[22] using an EPC7 amplifier (HEKA Instruments Inc., Bellmore, NY). Recordings were performed 24−72 h after passage or 24−48 h after transfection, using pipettes (3−4 MΩ, TW150, WPI, Sarasota, FL) filled with 120 mM CsCl, 10 mM EGTA/Ca^{2+}, and 10 mM HEPES-KOH (pH 7.35). The external bath solution contained 150 mM NaCl, 2.8 mM KCl, 1.0 mM $CaCl_2$, and 10 mM HEPES-NaOH (pH 7.4). Data were digitized at a rate 2.5−5 times the total filter cutoff frequency and analyzed using laboratory software or with QuB (http://www.qub.buffalo.edu).

Agonists in this study included (+)-α-amino-3-hydroxy-5-methylisoxazole-4-proprioniate (S-AMPA) (Tocris Bioscience, Ellisville, MO), L-glutamate (Sigma-Aldrich), L-quisqualate, (Ascent Scientific LLC, Princeton, NJ, or Tocris Bioscience),

dx.doi.org/10.1021/bi3001837 | *Biochemistry* 2012, 51, 4015−4027

and kainate (Tocris Bioscience or Ascent Scientific). The non-NMDA antagonist used was 6-cyano-7-nitroquinoxaline-2,3-dione (CNQX) (Tocris Bioscience or Ascent Scientific). Stock solutions (10−100 mM) of GluA receptor agonists and CNQX were prepared in deionized distilled water with equimolar amounts of NaOH, and the pH was adjusted to 7.2−7.4. Cyclothiazide (CTZ) (Tocris Bioscience or Ascent Scientific) was prepared as a 50 mM stock solution in absolute methanol. All recording solutions contained 100−150 μM CTZ.

Agonist concentration−effect data were obtained for wild-type and mutant GluA3$_i$ receptors by applying them over a range of concentrations and normalizing their responses in each cell to the 10 mM glutamate response. Cell stability was usually assessed by repeating applications of 100 μM glutamate or 300 μM kainate during the recording. Drugs were applied at room temperature (20−22 °C) by slow bath perfusion through a Warner Instruments (Hamden, CT) MP-8 manifold to cells voltage-clamped at −60 mV. Concentration−effect data shown in Figure 2 were fit (Origin 7, OriginLab Corp., Northampton, MA) with the Hill equation:

$$I = I_{\text{agonist}_{\text{max}}} \frac{[\text{agonist}]^{n_H}}{[\text{agonist}]^{n_H} + (EC_{50})^{n_H}}$$

where I is the agonist-evoked current at [agonist], $I_{\text{agonist}_{\text{max}}}$ is the peak current at a saturating concentration of agonist, [agonist] is the concentration of the agonist, EC_{50} is the concentration of the agonist that elicits a half-maximal response, and n_H is the Hill coefficient.

Schild analysis[23] was performed to compare the binding affinity of the wild-type and D655A receptors for the competitive antagonist CNQX. CNQX was used near its 50% inhibition concentration (IC_{50}), which was determined against a concentration of agonist that did not fully saturate the receptor. The dose ratio (DR) values (Figure 4A) were determined from the shift in the agonist response curves produced in the presence of three different concentrations of CNQX that bracketed the IC_{50} values for wild-type and GluA3$_i$-D655A mutant receptors.

Outside-out macropatch recordings were used to determine on- and off-response time constants. Pipettes (1.5−3.0 MΩ) were filled with 135 mM CsF, 33 mM CsOH, 2 mM $MgCl_2$, 1 mM $CaCl_2$, 10 mM HEPES, and 11 mM EGTA, adjusted to pH 7.4 (CsOH). Cells and excised patches were bathed in (extracellular) solutions containing 150 mM NaCl, 2.5 mM KCl, 1.0 mM $CaCl_2$, and 10 mM HEPES (pH 7.4). Lightly pressurized (0.02−0.06 mPa) extracellular solutions (control or glutamate) were applied through a glass theta tube (2.0 mm diameter) (Harvard Apparatus, Holliston, MA), which produced two streams with a sharp interface between them.[24] Theta tubes were treated with concentrated hydrofluoric acid for 20−25 min to decrease the thickness of the septum. Each barrel of the theta tube was connected to three solutions through a micromanifold controlled with pinch valves (VC6, Warner Instruments). The recording pipet containing the excised patch was positioned within a stream of control solution close to the interface. The theta tube was moved from position 1 to 2 so the second stream (containing one of two different glutamate solutions with 100−200 μM CTZ) was applied to the patch and returned to position 1 using a piezoelectric mechanical translator (Burleigh LSS-3100/3200), allowing for measurement of the on- and off-response time constants. Currents were low-pass filtered at 2, 5, or 10 kHz (Axopatch 200B, 4-pole Bessel), sampled at 10 or 50 kHz (Digidata, 1440A, Molecular Devices, Sunnyvale, CA) using pClamp version 10.2. Each trial included a 50 ms prepulse of control solution, followed by a 2.5 or 5 s application of glutamate with CTZ, followed by control solution for 14 s. Control solution was applied continuously to the patch while the agonist solution for the next trial was preloaded into the other barrel during the unrecorded 100 s interval between trials. CTZ-containing control solution was applied to the patch for 30 s at the end of the 100 s interval, prior to initiation of the next drug trial. All CTZ-containing solutions were made fresh every 2 h to ensure that desensitization did not interfere with the measurements.

Agonist application velocity was deduced by open-tip potential measurements made at the end of each recording using a 50% dilute control solution in the agonist application barrel. Data were included in Figure 6C if the 10−90% exchange occurred within 0.3 ms. Macropatch current traces were analyzed with Clampfit version 10.2, and the on (a) and off (b) responses were fit with a single-exponential function:

$$y = y_o + A_1(1 - e^{-x/\tau}) \quad \text{(a)}$$

$$y = y_o + A_1 e^{-x/\tau} \quad \text{(b)}$$

where y_o represents the y offset, A_1 the amplitude, and τ the time constant (pClamp version 10.2). Note that the value of τ is a relaxation (eigenvalue) that does not necessarily correspond to an individual rate constant in a kinetic mechanism. When peak currents were less than −10 pA, three to eight data traces were averaged before fitting.

Radioligand Binding. The soluble LBD domains of wild-type, GluA3-D655A, and GluA3-K660A receptors were expressed and purified as described by Chen et al.[25] and Ahmed et al.[17] Binding to isolated LBD proteins was performed in a buffer containing 30 mM HEPES, 100 mM KSCN, and 2.5 mM $CaCl_2$ with 10% glycerol (pH 7.2) (with NaOH). All solutions were maintained at 4 °C. Glutamate was removed from the LBD proteins by successive concentration and dilution in buffer, and protein was diluted to a final concentration of ∼2 nM. After the addition of [^{3}H]AMPA (46 Ci/mmol) (Perkin-Elmer, Waltham, MA), the reaction (200 μL in duplicate) with competing ligands (AMPA, CNQX, glutamate, kainate, and quisqualate) proceeded for 1 h followed by filtration of the mixture with GSWP filters (Millipore, Bedford, MA) and two 2 mL washes with binding buffer. Analysis was done using Kaleidagraph (Synergy Software, Reading, PA). Competition for binding of [^{3}H]AMPA with unlabeled AMPA was used to determine changes in AMPA affinity and to convert the IC_{50} values to K_i values according to the Cheng−Prusoff equation.[26]

Thermal Stability. Intrinsic tryptophan fluorescence measured with a Varian Cary Eclipse spectrofluorimeter (excitation wavelength of 280 nm and emission wavelength of 336 nm) was used to measure thermal unfolding. The temperature was monitored continuously and changed at a rate of 0.06 °C/min from 10 and 70 °C. For the measurements, protein was diluted to 1−2 μM in 10 mM glutamate, 25 mM sodium acetate (pH 6.0), 25 mM sodium chloride, and 1 mM sodium azide. Data were analyzed using Kaleidagraph (Synergy Software) as described by Madden et al.[27]

Structural Analysis. For crystallization trials, the proteins were concentrated to 0.2−0.5 mM using a Millipore Centricon 10 centrifugal filter. Ligands were exchanged into the sample by

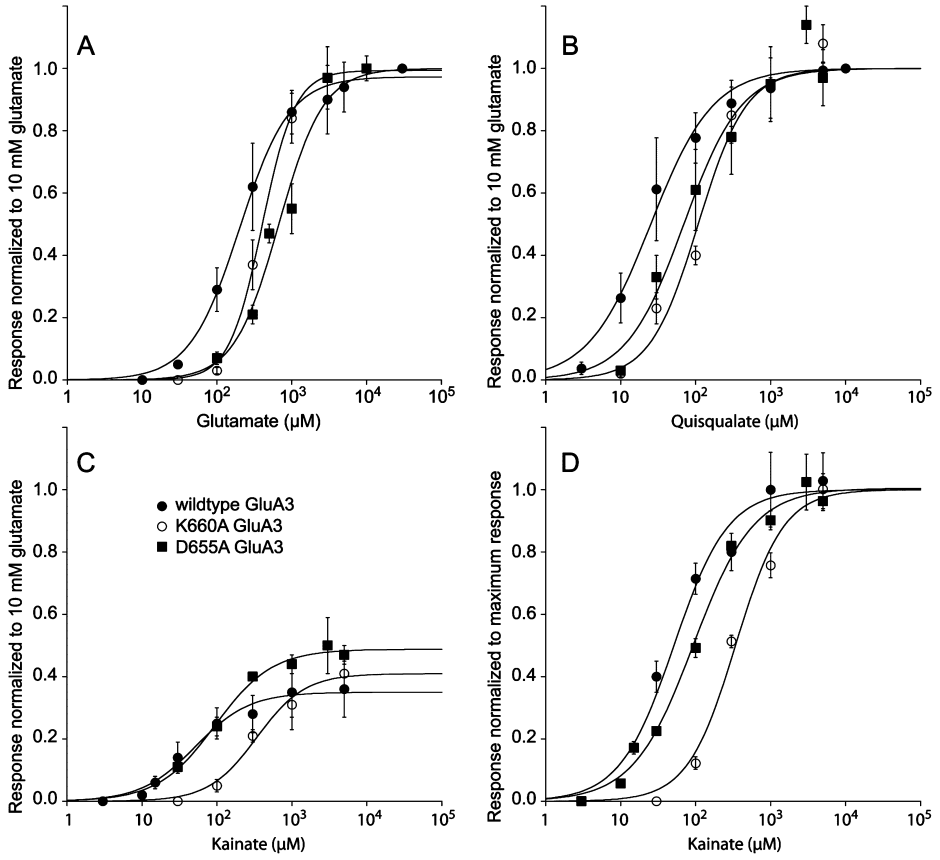

Figure 2. D655A and K660A mutations affect agonist function. (A) Glutamate concentration−effect relationships for wild-type $GluA3_i$ (■), $GluA3_i$-D655A (□), and $GluA3_i$-K660A (○). Response curves of mutant receptors are shifted to the right. (B) A similar pattern of changes was seen in the quisqualate response curves. (C) Kainate was a partial agonist for all three receptors. Kainate efficacy, measured relative to the response to the 10 mM glutamate response in the same cells, increased significantly ($p < 0.5$) for the D655A mutant compared to the wildtype. (D) Normalizing the kainate concentration−effect curves to the maximal kainate response obtained (5 mM $GluA3_i$-D655A) illustrates the small rightward shift of the response curve of $GluA3_i$-D655A compared to wild-type $GluA3_i$. Cells (3−15 per agonist concentration) were held at −60 mV, and agonist responses (A−C) were normalized to the response to 10 mM glutamate (bars give means ± the standard deviation). CTZ (100−150 μM) was present in all recordings. EC_{50} values and Hill slopes are listed in Table 1.

successive concentration [Amicon Ultra-4 (10K) filter] and dilution using buffer in the first eight steps followed by four washes in the presence of ligand. The final protein concentration was approximately 0.3 mM. The final ligand concentrations were 10 mM for L-glutamate, 5 mM for kainate and CNQX, and 2 mM for quisqualate. All crystals were grown at 4 °C using the hanging drop technique, and the drops contained a 1:1 (v/v) ratio of protein solution to reservoir solution. In all cases, the reservoir solution consisted of 15−16% polyethylene glycol (PEG) 8K, 0.05−0.1 M sodium cacodylate, 0.25 M ammonium sulfate, and 0.1 M zinc acetate (pH 6.5). Both flip ($GluA3_i$) and flop ($GluA3_o$) variants were tested, and those providing crystals with satisfactory refraction are reported.

Data were collected at Cornell High Energy Synchrotron Source beamline A1 using a Quantum-210 Area Detector Systems charge-coupled device detector. Data sets were indexed and scaled with HKL-3000.[28] Structures were determined with molecular replacement using Phenix.[29] Refinement was performed with Phenix,[29] and Coot 0.7[30] was used for model building. The domain orientation was determined as described by Gill et al.[18] Orientations are reported as closures or openings relative to the structure of $GluA3_i$ bound to glutamate reported previously [Protein Data Bank (PDB) entry 3dln[17]].

RESULTS

Functional Effects of the Loss of the Asp−Lys Salt Bridge. The pharmacological profile of wild-type $GluA3_i$ receptor channels was compared to those of $GluA3_i$-D655A and $GluA3_i$-K660A mutant receptors expressed in HEK293 cells in the presence of 100−150 μM CTZ, which suppresses desensitization of flip splice variant GluA receptors[31] and slows deactivation.[32] Agonist-dependent functional differences between the wild type and mutants are illustrated in Figure 2 and Figure S1 of the Supporting Information. Cells exposed to glutamate (10 mM) and quisqualate (5 mM) gave similar maximal current responses, while kainate (5 mM) was a partial agonist. Concentration−effect curves fitted with the Hill equation showed that the Hill slope increased in both D655A and K660A mutants for glutamate from 1.3 (wild type) to 1.5 (D655A) to 2.0 (K660A). EC_{50} values for all three agonists were increased for the mutants relative to that of the wild type (Figure 2A,B,D), but the magnitude of the EC_{50} shifts differed among the agonists (Table 1). The D655A mutation had its strongest effect on glutamate's EC_{50} and its weakest effect on kainate's, while the K660A mutation was the opposite. Kainate's efficacy was increased relative to that of glutamate in the D655A mutant [$p < 0.05$; 36 ± 2% in the wild type ($n = 9$) compared to 48 ± 6% ($n = 6$) for the D655A mutant]. This

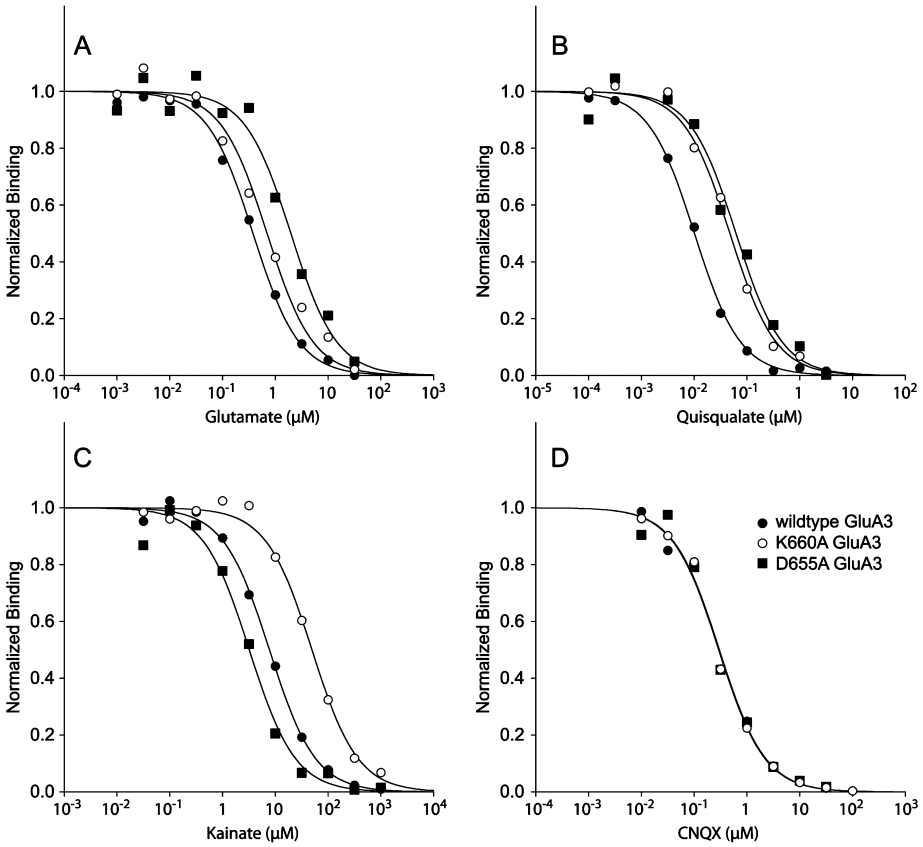

Figure 3. Agonist binding affinity, but not CNQX affinity, was affected by D655A and K660A mutations in the GluA3 LBD. Inhibition of the specific binding of the high-affinity agonist [^{3}H]AMPA by increasing concentrations of (A) glutamate, (B) quisqualate, (C) kainate, and (D) CNQX is shown in wild-type (■), D655A (□), and K660A (○) LBDs. IC_{50} values for glutamate and quisqualate increased for D655A and K660A compared to that of the wildtype. Kainate's IC_{50} increased in K660A relative to that of the wildtype, and IC_{50} values for CNQX were similar in the wild type and D655A and K660A mutants. AMPA affinity (data not shown) was decreased for the D655A and K660A mutations by ~2-fold. K_i values listed in Table 1 show that kainate affinity was unchanged by the D655A mutation and CNQX binding affinity was the same for all three receptors.

difference in kainate efficacy did not appear to be due to a change in steady-state desensitization because kainate responses from cells expressing wild-type and $GluA3_i$-D655A receptor channels were potentiated to the same extent by 30, 100, and 300 μM CTZ (Figure S1 of the Supporting Information).

Binding Affinity Is Decreased for Agonists but Not for the Antagonist CNQX. We investigated the binding affinity of the agonists used in the EC_{50} studies in the isolated LBD for wild-type and mutant receptors because an increase in EC_{50} in a holo receptor can arise from a decrease in the intrinsic binding affinity for ligands, or from changes subsequent to binding due to conformational changes reflecting receptor activation and/or deactivation kinetics. Competition binding assays for several ligands were performed with purified preparations of wild-type, GluA3-D655A, and GluA3-K660A LBD proteins using [^{3}H]AMPA to determine IC_{50} values (Figure 3 and Table 1). Both mutations decreased AMPA affinity by ~2-fold (K_i values increased), and the affinity of glutamate and quisqualate also decreased in the D655A (7.6- and 8.4-fold, respectively) and K660A (2.5- and 6-fold, respectively) mutants compared to that of the wildtype. The binding results for kainate followed a different pattern (Figure 3C). While the K_i for kainate was essentially unchanged in the D655A mutant relative to that in the wildtype, it increased by nearly 10-fold in the K660A mutant, which is consistent with the larger shift in kainate's EC_{50} in the K660A mutant. While the affinity of full agonists decreased significantly, competition against [^{3}H]AMPA using the antagonist CNQX produced nearly identical curves for the wildtype and both mutants (Figure 3D), and the K_i values for CNQX were similar in wild-type and D655A and K660A mutant LBDs.

Table 1 summarizes pharmacological parameters, including EC_{50}, IC_{50}, and K_i values for the wildtype and the mutant GluA3 receptors (Figures 2 and 3). Function-to-binding ratios (EC_{50} or K_b to K_i) were calculated to facilitate comparisons between the different assays.[42] In wild-type GluA3, the ratio was <10 for CNQX, 15 for kainate, ~1200 for glutamate, and 5000 for quisqualate (Figure 4A). There is a large difference between agonist potency (EC_{50}) and binding affinity (K_i) for full agonists, while for the partial agonist kainate, where the activation of the channel is less probable, the EC_{50} to K_i ratio was much smaller. For the competitive antagonist CNQX, we compared the K_b obtained from Schild analysis (see below) to the K_i ratio and found the ratio was less than 10. In the mutant receptors, the increase in K_i was greater than the change in EC_{50} for glutamate and quisqualate in the D655A mutant (Figure 4B). For kainate, K_i was not significantly changed in the D655A mutant, but the EC_{50} increased, which increased the potency:affinity ratio by 3-fold. In the K660A mutant, the K_i and EC_{50} values increased a comparable amount for kainate, maintaining the relationship between potency and binding affinity.

CNQX Action and Affinity Unchanged by the D655A Mutation. Previous studies reported that some mutations in

dx.doi.org/10.1021/bi3001837 | *Biochemistry* 2012, 51, 4015−4027

Table 1. Pharmacologic Parameters of Wild-Type and Mutant Holo Receptors and LBDs[a]

	EC_{50} (μM)	efficacy[b]	Hill number	IC_{50}[c] (μM)	K_i (μM)	EC_{50}/K_i
AMPA						
wildtype	ND	–	–	0.006	0.009[e]	–
D655A	ND	–	–	0.024	0.020	–
K660A	ND	–	–	0.029	0.0173	–
quisqualate						
wildtype	25 ± 7	1	1.0	0.010 ± 0.000	0.005	5000
D655A	69 ± 14	1	1.1	0.062 ± 0.008	0.042	1643
K660A	108 ± 9	1	1.4	0.047 ± 0.004	0.030	3600
glutamate						
wildtype	201 ± 55	1	1.3	0.379 ± 0.022	0.168	1196
D655A	672 ± 73	1	1.5	1.970 ± 0.287	1.271	529
K660A	403 ± 14	1	2.0	0.699 ± 0.090	0.427	944
kainate						
wildtype	56 ± 18	0.35	1.2	7.75 ± 0.44	3.44	16
D655A	94 ± 9	0.48	1.1	3.22 ± 0.40	2.08	45
K660A	340 ± 50	0.41	1.4	49.5 ± 4.10	30.26	11

	K_b[d]					K_b/K_i
CNQX						
wildtype	0.96	–	–	0.295	0.139	7
D655A	1.00	–	–	0.301 ± 0.033	0.191	5
K660A	ND	–	–	0.294 ± 0.028	0.187	–

[a]Errors are the standard errors of the mean. [b]Relative to glutamate. [c]Ligand binding. [d]K_b from Schild analysis. [e]The K_d from AMPA direct binding was used to calculate K_i values of other ligands in the wild-type GluA3 LBD.

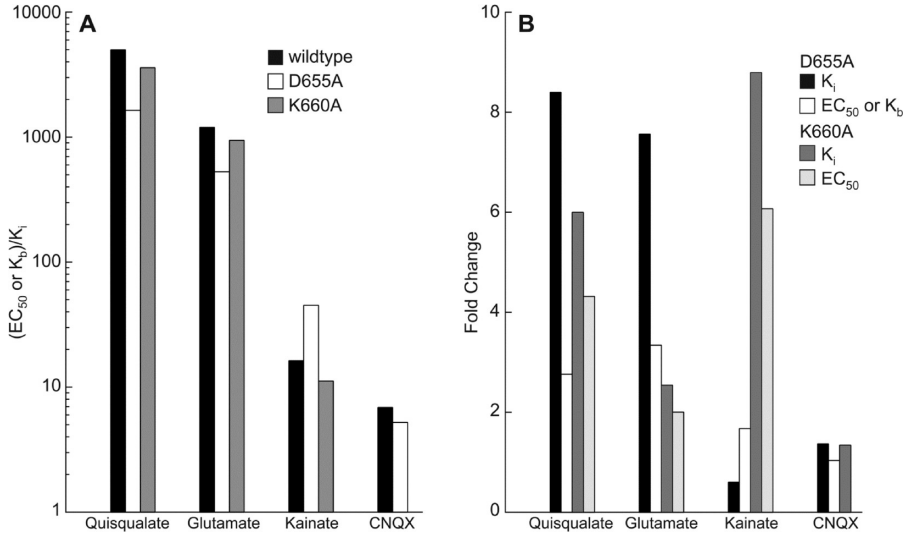

Figure 4. Relationship between ligand potency (EC_{50} or K_b) and ligand binding affinity (K_i) in the mutants is ligand-dependent. (A) The ratio between the potency of the ligand (EC_{50} or K_b) in the holo receptor to the ligand K_i measured in isolated LBDs reported in Table 1 is plotted for the wild-type, GluA3-D655A, and GluA3-K660A receptors. The log difference between functional potency and binding affinity was smallest for the antagonist CNQX and greatest for the highest-affinity agonist quisqualate in wild-type and mutant receptors. (B) Bars represent the fold change in potency and affinity values for mutant receptors compared to those of the wildtype. Greater differences for affinity changes than potency changes were seen for full agonists in the D655A mutant than for the partial agonist kainate and the antagonist CNQX. The K660 mutant showed a different agonist-dependent pattern of changes in affinity and potency compared to that of the D655A mutant.

GluA receptors convert CNQX to a partial agonist.[33] The mechanism of inhibition and the affinity for an antagonist can be determined in a functional assay without kinetic modeling by performing Schild analysis[34−37] using an antagonist that occupies the same binding site as agonists and makes many of the same contacts. In the GluA2 LBD, CNQX was shown to occupy the same site as agonists.[38] To verify that this was also the case for GluA3, we determined the structure of $GluA3_i$ bound to CNQX [1.8 Å (Figure S2 and Table S1 of the Supporting Information)] and found that the structure was very similar to that determined for GluA2 (the lobe opening relative to $GluA3_i$ bound to glutamate for the GluA2−CNQX complex was 13.8 ± 0.04° and for the $GluA3_i$−CNQX complex was 13.3 ± 0.6°). Neither wild-type nor $GluA3_i$-D655A receptor channels responded to direct application of 0.2−20 μM CNQX (data not shown). It was a fully reversible inhibitor of glutamate-evoked responses in wild-type and $GluA3_i$-D655A receptor channels so it was used to obtain concentration−

dx.doi.org/10.1021/bi3001837 | *Biochemistry* 2012, 51, 4015−4027

inhibition curves against 200 μM glutamate in wild-type GluA3$_i$ and 1600 μM glutamate in GluA3$_i$-D655A receptors. IC_{50} values for CNQX were 1.5 ± 0.3 and 1.2 ± 0.3 μM for the wildtype and mutant, respectively. These parameters were used to design the protocol for the Schild analysis (Figure S3 of the Supporting Information). Partial glutamate concentration−effect curves were obtained in the presence of 0.2, 1.0, and 2.0 μM CNQX for the wild type and GluA3$_i$-D655A. Figure 5A shows the slopes of these curves were unchanged in CNQX. Dose ratio (DR) values, calculated from the shifts in the glutamate concentration−effect curves for the wild-type and D655A mutant receptors (Figure 5A), were plotted against the CNQX concentration in Figure 5B (Schild plot). The log-linear slopes were 0.88 and 0.86 for the wild type and D655A mutant, respectively, indicating that CNQX is a competitive antagonist in the mutant and wild-type receptors. By convention, the data were refitted with a fixed slope of 1.0 to yield the affinity for CNQX (K_b), which was 0.96 μM in the wildtype and 1.0 μM in the GluA3$_i$-D655A mutant receptor. Thus, functional analysis indicated that the CNQX affinity was unchanged by the D655A mutation.

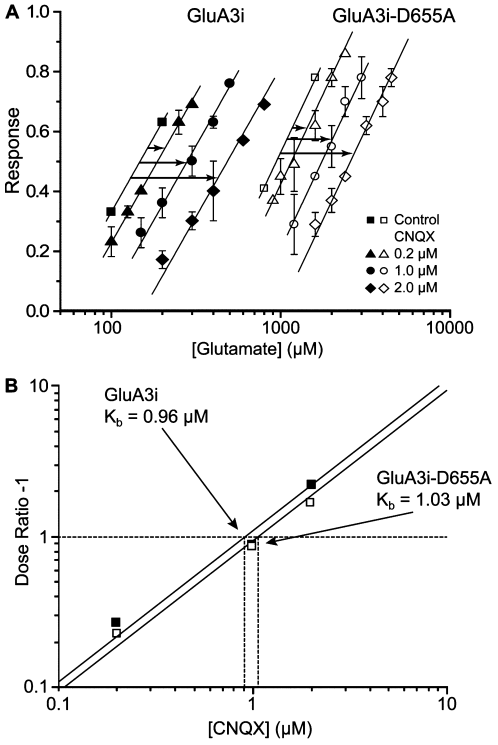

Figure 5. Wild-type and GluA3$_i$-D655A receptor channels had similar affinity for CNQX. (A) Partial glutamate concentration−effect curves were obtained using whole cell currents recorded from cells expressing the wild type (filled symbols) and the mutant GluA3$_i$ (empty symbols), in the absence and presence of the antagonist CNQX. Each data point represents two to eight cells (mean ± standard error of the mean; 2−11 trials per cell). Dose ratios (DRs) were determined from the rightward shift of the concentration−effect curves (arrows) at increasing concentrations of CNQX. (B) Schild plots of log[DR-1] vs log[CNQX] for wild-type and GluA3$_i$-D655A data were both fitted by lines with a slope of 1, indicating competitive antagonism. The CNQX functional affinity (K_b) was unchanged.

It is noteworthy that the ratio of the CNQX K_b determined in the holo receptors to the K_i determined in the isolated LBDs was <10, indicating that the functional affinity and binding affinity are very similar. In contrast, full agonists have very large EC_{50}/K_i ratios, which were decreased in the mutants but remained at least 2 orders of magnitude larger than the K_b/K_i ratio for CNQX (Figure 4A). The high ratios observed for the full agonists most likely stem from the block of desensitization by cyclothiazide for EC_{50} measurements, while the K_i measured in LBD binding assays is the thermodynamic equivalent of an agonist-induced desensitized receptor conformation. This interpretation is also consistent with the kainate data, because this partial agonist does not completely desensitize wild-type or GluA3$_i$-D655A receptor channels (Figure S1D,E of the Supporting Information), and it has an EC_{50}/K_i ratio closer to that of CNQX than to that of the full agonists [<50 vs >1000 for glutamate (Table 1)].

Glutamate Response Activation Is Slower in Both Mutants. In the isolated LBD, the binding affinity of CNQX for either the D655A or the K660A mutant was unchanged compared to that for the wildtype, as was the affinity determined by Schild analysis measuring responses in the GluA3$_i$-D655A mutant receptor channels. This suggests that at least the initial step of ligand binding, the docking of the ligand in lobe 1, is not affected by these mutations.

We investigated the effects of the D655A and K660A mutations on response kinetics by rapidly applying glutamate to excised membrane patches (Figure 6A,B) using a piezoelectric mechanical translation device.[24] Despite measures to increase the level of receptor expression (see Materials and Methods), outside-out macropatches contained few channels and typically responses were small, particularly for the GluA3$_i$-D655A mutant.

When 1 mM glutamate and 5 mM glutamate were applied to patches containing the wildtype or the D655A mutant, the response amplitude increased as predicted by whole cell concentration−effect data (Figure 2) and response rise time decreased. Time constant values for the onset of the response (τ_{on}) in patches expressing wild-type GluA3$_i$ decreased from 5.5 ± 0.6 ms (n = 4) to 1.7 ± 0.2 ms (n = 4) to 0.8 ± 0.1 ms (n = 5) as the glutamate concentration increased from 1 mM to 5 mM to 10 mM, respectively (Figure 6C). τ_{on} was significantly longer for patches expressing GluA3$_i$-D655A mutant channels exposed to 1 mM glutamate (9.7 ± 0.8 ms; n = 5; p = 0.01) and 5 mM glutamate (6.9 ± 0.7 ms; n = 4; p = 0.02) than in the wild type. Responses of patches expressing GluA3$_i$-K660A receptors to 10 mM glutamate (τ_{on} = 3.2 ± 0.5 ms; n = 5) were significantly slower (p < 0.01) than that observed for wild-type GluA3$_i$ (τ_{on} = 0.8 ± 0.1 ms; n = 5).

The time constant for channel closing (τ_{off}) was measured for 5 and/or 10 mM glutamate in the wild type (τ_{off} = 3.4 ± 0.6 ms), GluA3$_i$-D655A (τ_{off} = 3.4 ± 0.3 ms), and GluA3$_i$-K669A (τ_{off} = 4.1 ± 1.0 ms). Upon comparison of the wild-type and mutant responses, the onset was faster for the wild type than for the mutants, and channel closing (deactivation) was unaffected. These results are consistent with a slowing of the activation rate, which includes the steps of ligand binding to lobe 1, which was not affected by antagonist binding according to the CNQX data, while agonist-induced receptor activation (lobe closure, Asp−Ser peptide flip, interlobe H-bond formation, and channel opening), for GluA3$_i$ receptor channels was affected when the D655−K660 salt bridge was lost.

The Thermal Stability of D655A and K660A Mutants Decreases Relative to That of Wild-Type LBDs. The thermal unfolding of the wild-type, D655A, and K660A GluA3$_i$ LBDs bound to glutamate was measured with intrinsic

dx.doi.org/10.1021/bi3001837 | Biochemistry 2012, 51, 4015−4027

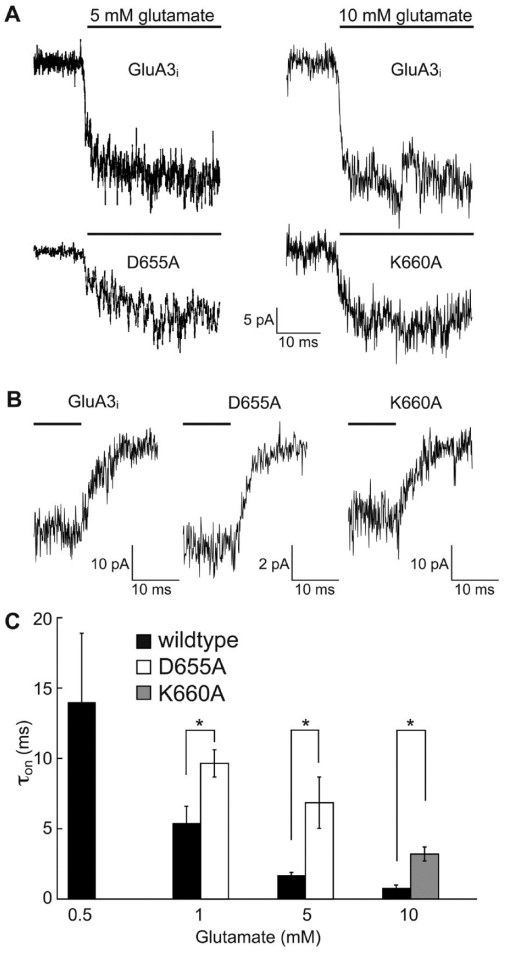

Figure 6. Glutamate response activation is slower in D655A and K660A mutants. (A) Traces show responses from outside-out macropatches exposed to rapid application of glutamate (5 and 10 mM) to patches containing $GluA3_i$ (top) and the D655A and K660A mutant (bottom) receptor channels. (B) Off responses of wild-type (left), D655A (center), and K660A (right) receptors obtained after switching to control solution. (C) τ_{on} values for activation of $GluA3_i$ (black), D655A (white), and K660 (gray) receptor channel responses show the influence of an increasing glutamate concentration. Wild-type receptors were activated faster at all concentrations, including 10 mM glutamate, which produces maximal amplitude responses for wild-type and mutant receptors (see Figure 2). Data were taken from 23 patches held at −100 mV.

tryptophan fluorescence. The increase in temperature from 10 to 70 °C resulted in a linear decrease in fluorescence overlaid with a transition associated with protein unfolding (Figure S4 of the Supporting Information). Both mutants were less stable than the wildtype, with T_m values of 49.1, 52.6, and 57.1 °C for D655A, K660A, and the wildtype, respectively.

Crystal Structures of the Wild-Type and D655A Mutant LBDs. Crystal structures of glutamate-, quisqualate-, and kainate-bound wild-type and GluA3-D655A mutant LBDs and the kainate-bound K660A mutant were determined to investigate whether these mutations altered the protein structure bound to the different agonists. Despite repeated attempts, crystals obtained for the K660A mutant bound to quisqualate and glutamate did not refract sufficiently well to obtain a structure. The structures of the binding sites are presented in Figures 7 and 8, and structural statistics are listed in Table S1 of the Supporting Information.

Wild-Type Structures. The structures of wild-type $GluA3_i$ (PDB entry 3dln;[17] 1.91 Å) and $GluA3_o$ (PDB entry 3m3k;[39] 1.79 Å) LBDs bound to glutamate were reported previously. The $GluA3_i$ LBD had one structure in the asymmetric unit with a flipped peptide bond (Figure 7A,C). $GluA3_o$ had three structures in the asymmetric unit, and the peptide bond was flipped in all three cases. Relative to $GluA3_i$, the lobe orientation of the three structures of $GluA3_o$ was 1.9 ± 0.6° more closed. The structure of $GluA3_i$ bound to quisqualate was determined to 1.7 Å, with one structure in the asymmetric unit. A second structure was also determined to 1.75 Å but was essentially identical to the first, so only one is described in Table S1 of the Supporting Information. In both cases, the D655−S656 peptide bond was flipped (Figure 7D,F). The structures had lobe orientations essentially the same as those of $GluA3_i$ bound to glutamate. Two wild-type structures of the $GluA3_i$ LBD bound to kainate were determined to 1.8 and 2.2 Å resolution (Figure 8A,D and Table S1 of the Supporting Information). The lobe 1−lobe 2 cleft closure of wild-type $GluA3_i$ bound to kainate (6.1 ± 0.45°) was similar to that of the GluA4 kainate-bound structure (5.8°)[18] and greater than that of GluA2 (8.8°).[13] At least part of the reason for this is that the terminal methyls of L654 are rotated by 180° in both GluA3 and GluA4, allowing the lobes to move closer together. Gill et al.[18] also attributed the closer approach of the two lobes to phenylalanine at position 703 in GluA4 (F706 in GluA3) versus tyrosine in GluA2. The loss of the hydroxyl in GluA4 results in a loss of one of two waters that form a H-bond network to kainate. As in GluA2 and GluA4, the D6556−S656 peptide bond is not flipped in any GluA3 structures bound to kainate (Figure 8).

D655A−Glutamate Complex. We obtained structures of the D655A mutant $GluA3_o$ LBD bound to glutamate for four separate crystals [1.8−1.9 Å (Table S1 of the Supporting Information)]. The structures did not differ significantly, so only one is reported in Table S1 of the Supporting Information. In all cases, the A655−S656 peptide bond was unflipped (Figure 7B,C). The lobes were open by 2.8 ± 0.2° relative to that of wild-type $GluA3_i$. The effect of the D655A mutation seems to be twofold. First, the salt bridge with K660 is lost, and second, the tendency to form H-bonds across the lobe interface may be weakened. The decrease in the propensity to form the H-bonds is likely due to the fact that the backbone carbonyl of the residue at position 655 can also rotate to interact with the side chain of K660. In this orientation, the peptide bond is not flipped and the H-bonds cannot form in the D655A mutant, thus stabilizing the unflipped conformation of the peptide bond upon removal of the salt bridge.

D655A−Quisqualate Complex. For the D655A mutant, two structures were obtained for the $GluA3_o$ LBD bound to quisqualate from different crystals (1.8 and 2.2 Å), but there was only one copy in each (Figure 7E,F and Table S1 of the Supporting Information). In both cases, the A655−S656 peptide backbone appeared to be flipped, but the density was weaker than that of the remainder of the protein (Figure 7F, right). In one structure, the hydrogen bonding pattern (A655−H_2O−Y452; S656−G453) was clearly present; however, the A655−H_2O−Y452 H-bond was not observed in the other structure. In both cases, a flipped structure seemed to be most consistent with the data, but lower contours of the density map suggested that both flipped and unflipped conformations were likely present. The lobe orientation was the same for both the

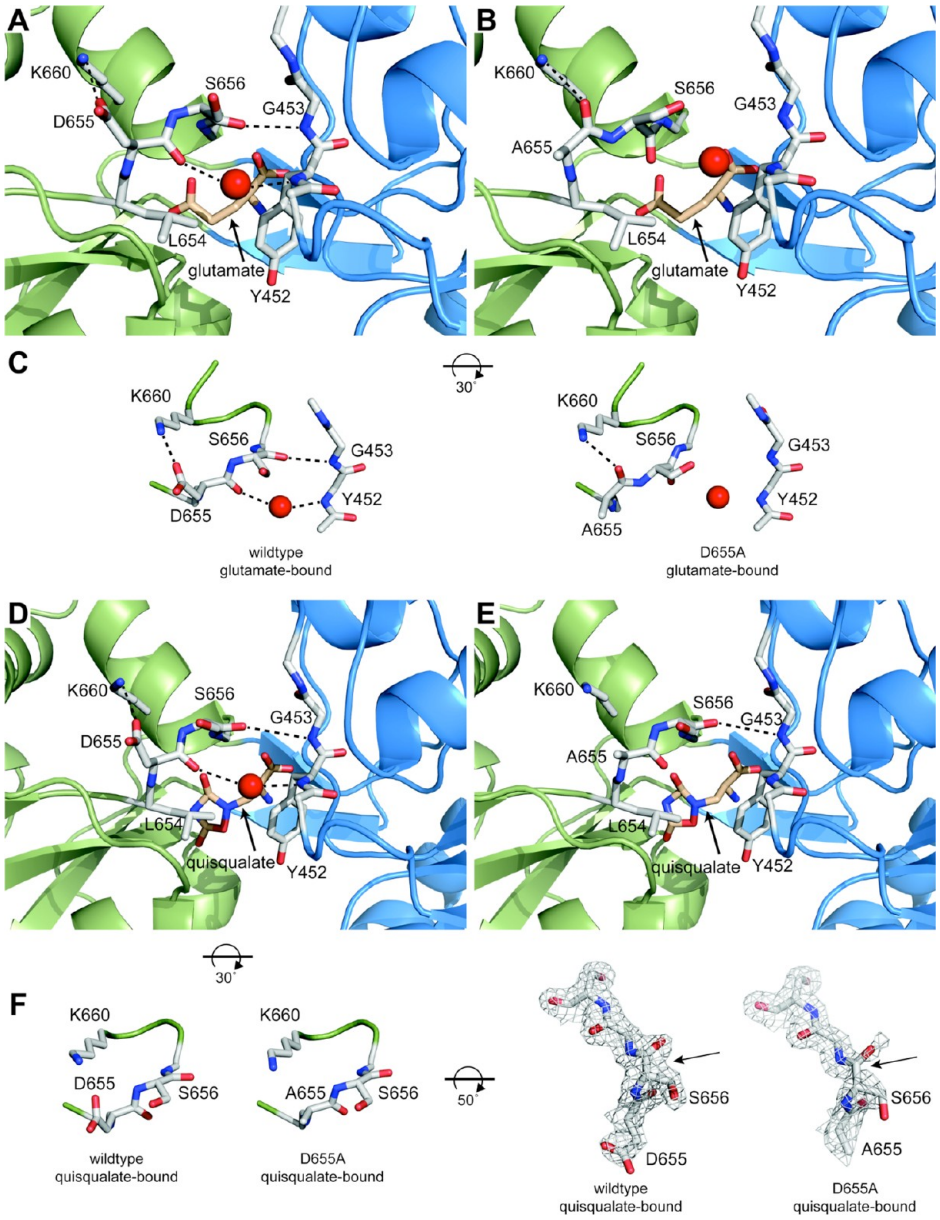

Figure 7. Binding sites for glutamate and quisqualate on the LBD of the wild-type (A and D) and D655A mutant (B and E) receptors. The wild-type GluA3 LBDs bound to glutamate (A and C) and quisqualate (D and F) are in the flipped conformation. In the GluA3-D655A mutant, the A655−S656 peptide bond is unflipped in the glutamate-bound form (B and C) and flipped in the quisqualate-bound form (E and F). However, the electron density maps in the quisqualate-bound form are weaker for the S656 backbone in the D655A mutant than in the wildtype (arrow in panel F). The representations in panel C and the left side of panel F are rotated 30° round the *x*-axis relative to panels A and B and panels D and E, respectively. For the electron density representation on the right side of panel F, the figure is rotated an additional 50° around the *x*-axis. Crystallographic water in the binding site is shown as a red sphere, and the residues involved in the peptide flip region and K660 are shown as sticks. Lobe 1 is colored cyan and lobe 2 green.

wildtype and the D655A mutant bound to quisqualate and did not differ from that of wild-type GluA3$_i$ bound to glutamate.

D655A−Kainate Complex. Two unique structures of kainate bound to the D655A mutant GluA3$_o$ LBD were found in the asymmetric unit [2.25 Å (Figure 8B,D)]. Like the wildtype, the A655−S656 bond was unflipped. The lobes of the two structures were open by 5.5 and 3.6 Å, respectively, relative to those of wild-type GluA3$_i$ bound to glutamate. One of the two structures was more closed than the wild-type structure, in part because of a greater rotation of the L654 side chain.

K660A−Kainate Complex. The structure of the GluA3-K660A LBD bound to kainate (Figure 8C) was refined to 2.1 Å (Table S1 of the Supporting Information). The L654 side chain was in the same orientation as in the wildtype (Figure 8C), and lobe 1−lobe 2 closure was similar to that of the wildtype bound to kainate (open by 5.6° relative to that of GluA$_i$ bound to glutamate). The side chain of D655 in the K660A mutant is rotated almost 180° around the β-carbon to point toward the cleft (Figure 8D). This may allow it to interact with the positively charged side chain of K688. The kainate-bound K660A mutation also shows a change in the E661−R664 salt bridge. The side chain of R664 moves in the direction of the lobe interface and occupies space that was vacated when K660 was replaced with alanine, and E661 moves away from the lobe

dx.doi.org/10.1021/bi3001837 | *Biochemistry* 2012, 51, 4015−4027

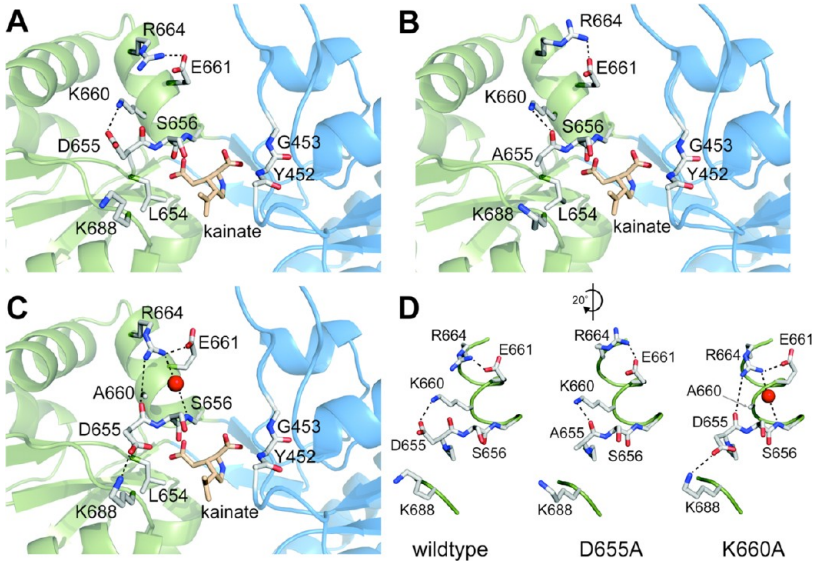

Figure 8. Binding sites for kainate on the LBD of wild-type, D655A, and K660A receptors. In all three proteins, the D655−S656 peptide bond was unflipped. (A) In the wild-type GluA3 LBD bound to kainate, both the side chain and backbone carbonyl of D655 can interact with the side chain in K660. Also, R664 forms a salt bridge with E661. The side chain of L654 can clash with the isoprenyl group of kainate to keep the lobes partially open, but studies of GluA2 show that it is possible for the side chain to rotate and the lobes to close fully, although presumably with low probability.[49] (B) In GluA3-D655A bound to kainate, the interaction between the side chain of position 655 and K660 is lost, but the carbonyl of A655 now interacts with the side chain of K660. In this structure, the side chain of L654 is rotated with respect to the wildtype and the lobes are slightly more closed (by 3°). (C) In GluA3-K660A bound to kainate, the electrostatics surrounding the binding site change significantly. A network of interactions involving the side chains of R664 and E661 and the backbone atoms of D655 and S656 replaces the simple salt bridge between R664 and E661. This is apparently due to the additional space and a change in charge as a result of the removal of the side chain of K660. The side chain of D655 rotates to interact with K688. L654 is in the same conformation as the wildtype, and the lobe closure is similar to that of the wildtype. The red sphere is a crystallographic water molecule. Lobe 1 is colored cyan and lobe 2 green. (D) Changes in the electrostatic interactions from the wildtype to the D655A and K660A mutants. The figures are rotated 20° around the *y*-axis relative to panels A−C.

1−lobe 2 interface. This also positions the side chain of R664 to interact with the carbonyl of D655 (Figure 8D). These changes may be responsible for the small twist of lobe 2 in the K660A mutant observed with kainate bound, which very likely stabilizes the unflipped conformation. These changes are consistent with the increase in kainate EC_{50} observed for this mutant.

DISCUSSION

$GluA3_i$ homomeric receptor channels expressed in HEK293 cells share features of the AMPA receptors expressed in the early stages of brain development,[40] including fast opening and closing rates[41] and high permeability to Ca^{2+}.[42] Defining the mechanism of activation of GluA receptors is critically important to understanding their regulation in health and disease. Sobolevsky et al.[43] provided a detailed structural analysis of the full GluA2 receptor channel (without the C-terminus) that showed that both the amino-terminal domains and LBDs form pairs of dimers. Linkers between the LBD and the M1 and M3 transmembrane helices connect the binding domain to the 4-fold symmetrical ion channel and participate in channel gating. Our study is focused on lobe 2 of the GluA LBD where the 180° rotation of a peptide bond between an Asp residue and the adjacent serine (D655 and S656 in GluA3) is proposed to play a role in AMPA receptor activation.[12,16] In GluA receptors, this Asp also makes an electrostatic contact with a Lys residue located in helix F of lobe 2 (D655 and K660 in GluA3), thus linking the flexible peptide flip domain to the hydrophobic core of lobe 2. Through a series of pharmacological and structural studies using the isolated GluA3 LBD and the holo receptor channel, we observed a relationship between agonist-dependent structural differences in receptors with mutations in the LBD and functional changes in the holo receptor. Our findings suggest the electrostatic interaction between the peptide flip Asp residue and Lys 660 may favor the rotation of the D655−S656 peptide bond and formation of two cross-cleft H-bonds that may allow a more efficient transfer of the energy of agonist-induced conformational changes to channel opening.

Neither the D655A nor the K660A mutation changed the binding affinity of the antagonist CNQX, and Schild analysis showed no change in the affinity of CNQX in $GluA3_i$-D655A receptors relative to that of the wild type, indicating these mutations are unlikely to affect the docking of the ligand with lobe 1. Slower activation of $GluA3_i$-D655A and $GluA3_i$-K660A receptor channels without a change in response-off kinetics (Figure 6) indicates that one or more of the steps leading to channel opening are affected by the mutations. The increase in the Hill slopes of the glutamate and quisqualate response curves, which was more apparent in $GluA3_i$-K660A receptors, suggests that activation of partially bound tetrameric mutant receptors may be less likely than in wild-type $GluA3_i$. A full interrogation of the differences in channel gating of these mutants will require rigorous systematic single-channel analysis, which will be challenging given the complexity of AMPA receptor channel gating.[44−47]

Structural Correlates of GluA Activation. The activation of ligand-gated receptors involves a series of conformational changes that starts with the initial interaction of the agonist with the receptor and ends with the opening of a permeation pathway. At least three conformational changes associated with GluA channel activation occur within the LBD: (1) diffusion of

dx.doi.org/10.1021/bi3001837 | *Biochemistry* 2012, 51, 4015−4027

the ligand and docking with lobe 1, (2) closure of the lobes and interaction of the ligand with lobe 2, and (3) formation of H-bonds across the lobe interface, which involves D655 and S656.[16]

CNQX functioned as a competitive antagonist (Figure 5). Crystal structures with CNQX show it interacts with lobe 1 and to some extent with lobe 2 (Figure S2 of the Supporting Information), but only rarely is lobe closure observed with CNQX bound.[48] The effects of the mutations were only minimal on CNQX affinity measured in the radioligand binding assay for both mutants, and in the Schild analysis of the wild-type and D655A holo receptors.

Kainate can progress through all three states, but like in CNQX, full closure of the lobes and formation of H-bonds across the interface are relatively rare events.[48] The D655A mutation did not affect binding of kainate to the LBD and had only a small effect on the EC_{50}. In contrast, the K660A mutation affected both binding and EC_{50} to a much greater extent, which is most likely due to the changes in the electrostatic interactions of D655 with K688 and R664 (Figure 8C).

Rapid application of glutamate revealed that the response on rate was slower for the mutants while the off rate was unchanged. The question is, at which step or steps from ligand docking in lobe 1 through to channel opening do these mutations slow the activation process that occurs with glutamate. Because CNQX affinity and function were not affected, the differences observed for quisqualate and glutamate in these mutants most likely stem from changes during and after closure of the lobes around the agonist and not during the initial binding step. Whole cell recordings showed the effect on glutamate EC_{50} was greater in the D655A mutant than in the K660A mutant, while both $GluA3_i$-D655A and $GluA3_i$-K660A receptor channel activation was slower for glutamate in the excised patches, indicating the mutations do not produce equivalent effects. Likewise, the thermal stability of $GluA3_i$ bound to glutamate was decreased in both mutants, D655A being less stable than K660A. The structural changes causing weakened glutamate function in the D655A mutant are consistent with a decreased stability of the "flipped" conformation of the D655A−S656 peptide bond in the mutant, which in the wild-type GluA3 LBD would otherwise make interlobe H-bonds. In the flipped conformation, the backbone carbonyl of D655 makes a water-mediated H-bond to the backbone amide of Y452, and the side chain of D655 interacts with the side chain of K660 in the wildtype. In the D655A mutant, the side chain interaction with K660 is eliminated, but the backbone carbonyl of A655 in the unflipped conformation can interact electrostatically with the side chain of K660. This would also stabilize the unflipped conformation of the backbone relative to the flipped conformation, perhaps further weakening the propensity to form the H-bond in the mutant. The crystal structures appear to be consistent with this interpretation, because when glutamate was bound the peptide bond was unflipped in the mutant but not in the wildtype. The effect of the D655A mutation on the quisqualate EC_{50} was weaker than that observed with glutamate, and in the crystal structure, the peptide bond was flipped with quisqualate bound; however, the electron density for D655 and S656 was decreased, suggesting motion between the two states. The functional changes observed for kainate in the D655A mutant were somewhat different. The shift in EC_{50} was smaller, and surprisingly, the efficacy of kainate measured relative to that of glutamate and quisqualate was increased. However, this result could also be explained if the efficacy of full agonists had decreased. The kainate-bound GluA3-D655A structure showed only a small change in lobe orientation relative to that of the wildtype, and the peptide bond was in the unflipped position in both cases. Moreover, the binding affinity for kainate in the isolated LBD was similar for the wildtype and the D655A mutant.

The crystal structure for the K660A mutant bound to kainate showed that the loss of the K660 side chain might also be expected to decrease the stability of the flipped conformation, because the side chain of D655 is no longer positioned away from the lobe interface by an electrostatic interaction with K660. In fact, in the kainate-bound K660A structure, the backbone carbonyl of D655 interacts with R664 in the unflipped conformation, and the side chain rotates toward the lobe interface and interacts with K688. There was a stronger effect of the K660A mutation on the kainate EC_{50} compared to those of the other agonists, and it was accompanied by a significant decrease in ligand binding affinity.

Even though the changes in the structures may explain the decrease in binding affinity and the slower channel response caused by these mutations, we cannot rule out the possibility that the slower activation observed in the mutants involves steps beyond the formation of the interlobe H-bonds and may involve structural rigidity within lobe 2. Maltsev et al.[49] has shown that lobe 2 consists of a β-sheet sandwiched between two hydrophobic cores. The connections between the hydrophobic cores and the β-sheet show dynamics on the microsecond to millisecond time scale. Thus, it is conceivable that the electrostatic interaction between K660 (within one hydrophobic core) and D655 is part of a system of electrostatic contacts that stabilizes lobe 2 and efficiently translates the energy of lobe closure to the linkers that connect the LBD to the ion channel domain of the protein. Severing one of these connections could weaken the link and perhaps slow the rate of activation.

CONCLUSIONS

We examined AMPA receptor activation with D655A and K660A mutations in a wild-type $GluA3_i$ background. Both mutations slowed glutamate-stimulated activation and produced modest changes in agonist binding affinity, while showing no effects on antagonist affinity or channel closing kinetics. Changes in the D655A mutant interlobe H-bond network for glutamate, kainate, and quisqualate correlated with observed EC_{50} changes and support the hypothesis that the peptide flip region plays a role in GluA activation. D655A and K660A mutations break an electrostatic contact with K660 in helix F, which tethers the peptide flip domain to helix F in wild-type receptors. Along with helix G, helix F is part of a hydrophobic core that has minimal additional interactions within the central β-sheet of lobe 2.[49] It is possible that the K660−D655 salt bridge is one of several electrostatic interactions that may contribute to rigidity in lobe 2 and permit efficient transduction of agonist binding energy to the ion channel linker.

ASSOCIATED CONTENT

Supporting Information

Examples of raw data traces from whole cell recordings used to generate the graphs in Figures 2 and 4 (Figures S1 and S3, respectively), the crystal structure of the GluA3 LBD with the

antagonist CNQX in the binding site (Figure S2), and the decrease in intrinsic fluorescence as the wild-type and mutated LBD proteins were heated (Figure S4). The parameters and statistics for fitting the crystal structures in Figures 7, 8 and S2 are provided in Table S1.This material is available free of charge via the Internet at http://pubs.acs.org.

AUTHOR INFORMATION

Corresponding Author

*Department of Molecular Medicine, C3-117 Veterinary Medical Center, Cornell University, Ithaca, NY 14853. Phone: (607) 253-3655. E-mail: lmn1@cornell.edu.

Present Address

§Department of Psychiatry and Biobehavioral Sciences, UCLA, Los Angeles, CA 90024.

Funding

This work was supported by a grant from the National Institutes of Health (R01 NS049223). It includes research conducted at the Cornell High Energy Synchrotron Source (CHESS), which is supported by the National Science Foundation under Grant DMR-0936384, using the Macromolecular Diffraction at CHESS (MacCHESS) facility, which is supported by Grant GM103485 from the National Institutes of Health, through its National Institute of General Medical Sciences.

Notes

The authors declare no competing financial interest.

ACKNOWLEDGMENTS

Dr. Stephen Heinemann provided the GluA3-flop cDNA, and Dr. James Eberwine provided the E14 mouse brain library and expert advice. Ms. Heather Larkin provided technical assistance. We thank Drs. George P. Hess, David Deitcher, Ronald Harris-Warrick, Huai-Hu Chuang, and Kinning Poon for helpful discussions.

ABBREVIATIONS

AMPA, α-amino-3-hydroxy-5-methyl-4-isoxazolepropionic acid; CNQX, 6-cyano-7-nitroquinoxaline-2,3-dione; CTZ, cyclothiazide [6-chloro-3,4-dihydro-3-(5-norbornen-2-yl)-2*H*-1,2,4-benzothiazidiazine-7-sulfonamide 1,1-dioxide]; FW, (*S*)-5-fluorowillardiine [(*S*)-(−)-α-amino-5-fluoro-3,4-dihydro-2,4-dioxo-1(2*H*)pyridinepropanoic acid]; GluA1−4, four subtypes of the AMPA receptor; $GluA2_o$, flop form of GluA2; $GluA3_i$, flip form of GluA3; GluK1−5, five subtypes of the kainate receptor; iGluR, ionotropic glutamate receptor; KA, kainate; LBD, extracellular ligand binding domain of GluA2 and GluA3; NMDA, *N*-methyl-D-aspartic acid.

REFERENCES

(1) Dingledine, R., Borges, K., Bowie, D., and Traynelis, S. (1999) The glutamate receptor ion channels. *Pharmacol. Rev. 51*, 7−61.

(2) Lee, Y. S., and Silva, A. J. (2009) The molecular and cellular biology of enhanced cognition. *Nat. Rev. Neurosci. 10*, 126−140.

(3) Cohen, S., and Greenberg, M. E. (2008) Communication between the synapse and the nucleus in neuronal development, plasticity, and disease. *Annu. Rev. Cell Dev. Biol. 24*, 183−209.

(4) Ghosh, A., Carnahan, J., and Greenberg, M. E. (1994) Requirement for BDNF in activity-dependent survival of cortical neurons. *Science 263*, 1618−1623.

(5) Citri, A., and Malenka, R. C. (2008) Synaptic plasticity: Multiple forms, functions, and mechanisms. *Neuropsychopharmacology 33*, 18−41.

(6) Derkach, V. A., Oh, M. C., Guire, E. S., and Soderling, T. R. (2007) Regulatory mechanisms of AMPA receptors in synaptic plasticity. *Nat. Rev. Neurosci. 8*, 101−113.

(7) Lau, C. G., and Zukin, R. S. (2007) NMDA receptor trafficking in synaptic plasticity and neuropsychiatric disorders. *Nat. Rev. Neurosci. 8*, 413−426.

(8) Liu, S. J., and Zukin, R. S. (2007) Ca^{2+}-permeable AMPA receptors in synaptic plasticity and neuronal death. *Trends Neurosci. 30*, 126−134.

(9) Heath, P. R., and Shaw, P. J. (2002) Update on the glutamatergic neurotransmitter system and the role of excitotoxicity in amyotrophic lateral sclerosis. *Muscle Nerve 26*, 438−458.

(10) Hynd, M. R., Scott, H. L., and Dodd, P. R. (2004) Glutamate-mediated excitotoxicity and neurodegeneration in Alzheimer's disease. *Neurochem. Int. 45*, 583−595.

(11) Steenland, H. W., Kim, S. S., and Zhuo, M. (2008) GluR3 subunit regulates sleep, breathing and seizure generation. *Eur. J. Neurosci. 27*, 1166−1173.

(12) Armstrong, N., and Gouaux, E. (2000) Mechanisms for activation and antagonism of an AMPA-sensitive glutamate receptor: Crystal structures of the GluR2 ligand binding core. *Neuron 28*, 165−181.

(13) Armstrong, N., Sun, Y., Chen, G. Q., and Gouaux, E. (1998) Structure of a glutamate-receptor ligand-binding core in complex with kainate. *Nature 395*, 913−917.

(14) Mayer, M. L. (2005) Crystal structures of the GluR5 and GluR6 ligand binding cores: Molecular mechanisms underlying kainate receptor selectivity. *Neuron 45*, 539−552.

(15) Furukawa, H., and Gouaux, E. (2003) Mechanisms of activation, inhibition and specificity: Crystal structures of the NMDA receptor NR1 ligand-binding core. *EMBO J. 22*, 2873−2885.

(16) Fenwick, M. K., and Oswald, R. E. (2010) On the mechanisms of α-amino-3-hydroxy-5-methylisoxazole-4-propionic acid (AMPA) receptor binding to glutamate and kainate. *J. Biol. Chem. 285*, 12334−12343.

(17) Ahmed, A. H., Wang, Q., Sondermann, H., and Oswald, R. E. (2009) Structure of the S1S2 glutamate binding domain of GluR3. *Proteins 75*, 628−637.

(18) Gill, A., Birdsey-Benson, A., Jones, B. L., Henderson, L. P., and Madden, D. R. (2008) Correlating AMPA receptor activation and cleft closure across subunits: Crystal structures of the GluR4 ligand-binding domain in complex with full and partial agonists. *Biochemistry 47*, 13831−13841.

(19) Grosman, C., Zhou, M., and Auerbach, A. (2000) Mapping the conformational wave of acetylcholine receptor channel gating. *Nature 403*, 773−776.

(20) Millhauser, G. L., Salpeter, E. E., and Oswald, R. E. (1988) Diffusion models of ion-channel gating and the origin of power-law distributions from single-channel recording. *Proc. Natl. Acad. Sci. U.S.A. 85*, 1503−1507.

(21) Huang, Z., Li, G., Pei, W., Sosa, L. A., and Niu, L. (2005) Enhancing protein expression in single HEK 293 cells. *J. Neurosci. Methods 142*, 159−166.

(22) Hamill, O. P., Marty, E., Neher, B., Sakmann, B., and Sigworth, F. J. (1981) Improved patch-clamp techniques for high-resolution current recording from cells and cell-free membrane patches. *Pfluegers Arch. 391*, 85−100.

(23) Verdoorn, T. A., Kleckner, N. W., and Dingledine, R. (1989) N-Methyl-D-aspartate/glycine and quisqualate/kainate receptors expressed in *Xenopus* oocytes: Antagonist pharmacology. *Mol. Pharmacol. 35*, 360−368.

(24) Amico-Ruvio, S. A., Murthy, S. E., Smith, T. P., and Popescu, G. K. (2011) Zinc Effects on NMDA Receptor Gating Kinetics. *Biophys. J. 100*, 1910−1918.

(25) Chen, G. Q., Sun, Y., Jin, R., and Gouaux, E. (1998) Probing the ligand binding domain of the GluR2 receptor by proteolysis and deletion mutagenesis defines domain boundaries and yields a crystallizable construct. *Protein Sci. 7*, 2623−2630.

(26) Cheng, Y., and Prusoff, W. H. (1973) Relationship between the inhibition constant (K_I) and the concentration of inhibitor which causes 50% inhibition (I_{50}) of an enzymatic reaction. *Biochem. Pharmacol. 22*, 3099−3108.
(27) Madden, D. R., Abele, R., Andersson, A., and Keinanen, K. (2000) Large-scale expression and thermodynamic characterization of a glutamate receptor agonist-binding domain. *Eur. J. Biochem. 267*, 4281−4289.
(28) Otwinowski, Z., and Minor, W. (1997) Processing of X-ray diffraction data collected in oscillation mode. In *Methods in Enzymology, Volume 276, Macromolecular Crystallography, Part A* (Carter, C. W., and Sweet, R. M., Eds.) pp 307−326, Academic Press, New York.
(29) Adams, P. D., Grosse-Kunstleve, R. W., Hung, L. W., Ioerger, T. R., McCoy, A. J., Moriarty, N. W., Read, R. J., Sacchettini, J. C., Sauter, N. K., and Terwilliger, T. C. (2002) PHENIX: Building new software for automated crystallographic structure determination. *Acta Crystallogr. D58*, 1948−1954.
(30) Emsley, P., and Cowtan, K. (2004) Coot: Model-building tools for molecular graphics. *Acta Crystallogr. D60*, 2126−2132.
(31) Partin, K. M., Patneau, D. K., and Mayer, M. L. (1994) Cyclothiazide differentially modulates desensitization of α-amino-3-hydroxy-5-methyl-4-isoxazoepropionic acid receptor splice variants. *Mol. Pharmacol. 46*, 129−138.
(32) Mitchell, N. A., and Fleck, M. W. (2007) Targeting AMPA receptor gating processes with allosteric modulators and mutations. *Biophys. J. 92*, 2392−2402.
(33) Taverna, F., Xiong, Z. G., Brandes, L., Roder, J. C., Salter, M. W., and MacDonald, J. F. (2000) The Lurcher mutation of an α-amino-3-hydroxy-5-methyl-4-isoxazolepropionic acid receptor subunit enhances potency of glutamate and converts an antagonist to an agonist. *J. Biol. Chem. 275*, 8475−8479.
(34) Colquhoun, D. (1998) Binding, gating, affinity and efficacy: The interpretation of structure-activity relationships for agonists and of the effects of mutating receptors. *Br. J. Pharmacol. 125*, 924−947.
(35) Colquhoun, D. (2007) What have we learned from single ion channels? *J. Physiol. 581*, 425−427.
(36) Schild, H. O. (1957) Drug antagonism and pAx. *Pharmacol. Rev. 9*, 242−246.
(37) Wyllie, D. J., and Chen, P. E. (2007) Taking the time to study competitive antagonism. *Br. J. Pharmacol. 150*, 541−551.
(38) Menuz, K., Stroud, R. M., Nicoll, R. A., and Hays, F. A. (2007) TARP auxiliary subunits switch AMPA receptor antagonists into partial agonists. *Science 318*, 815−817.
(39) Ahmed, A. H., Ptak, C. P., and Oswald, R. E. (2010) Molecular Mechanism of Flop Selectivity and Subsite Recognition for an AMPA Receptor Allosteric Modulator: Structures of GluA2 and GluA3 in Complexes with PEPA. *Biochemistry 49*, 2843−2850.
(40) Cull-Candy, S., Kelly, L., and Farrant, M. (2006) Regulation of Ca^{2+}-permeable AMPA receptors: Synaptic plasticity and beyond. *Curr. Opin. Neurobiol. 16*, 288−297.
(41) Pei, W., Huang, Z., and Niu, L. (2007) GluR3 flip and flop: Differences in channel opening kinetics. *Biochemistry 46*, 2027−2036.
(42) Varney, M. A., Rao, S. P., Jachec, C., Deal, C., Hess, S. D., Daggett, L. P., Lin, F., Johnson, E. C., and Velicelebi, G. (1998) Pharmacological characterization of the human ionotropic glutamate receptor subtype GluR3 stably expressed in mammalian cells. *J. Pharmacol. Exp. Ther. 285*, 358−370.
(43) Sobolevsky, A. I., Rosconi, M. P., and Gouaux, E. (2009) X-ray structure, symmetry and mechanism of an AMPA-subtype glutamate receptor. *Nature 462*, 745−756.
(44) Poon, K., Ahmed, A. H., Nowak, L. M., and Oswald, R. E. (2011) Mechanisms of Modal Activation of GluA3 Receptors. *Mol. Pharmacol. 80*, 49−59.
(45) Poon, K., Nowak, L. M., and Oswald, R. E. (2010) Characterizing single-channel behavior of GluA3 receptors. *Biophys. J. 99*, 1437−1446.
(46) Prieto, M. L., and Wollmuth, L. P. (2010) Gating modes in AMPA receptors. *J. Neurosci. 30*, 4449−4459.
(47) Zhang, W., Cho, Y., Lolis, E., and Howe, J. R. (2008) Structural and single-channel results indicate that the rates of ligand binding domain closing and opening directly impact AMPA receptor gating. *J. Neurosci. 28*, 932−943.
(48) Ahmed, A. H., Wang, S., Chuang, H. H., and Oswald, R. E. (2011) Mechanism of AMPA receptor activation by partial agonists: Disulfide trapping of closed lobe conformations. *J. Biol. Chem. 286*, 35257−35266.
(49) Maltsev, A. S., and Oswald, R. E. (2010) Hydrophobic side chain dynamics of a glutamate receptor ligand binding domain. *J. Biol. Chem. 285*, 10154−10162.